OPTIMISATION OF REAR CONTACT GEOMETRY OF HIGH-EFFICIENCY SILICON SOLAR CELLS USING THREE DIMENSIONAL NUMERICAL MODELLING

Gernot Heiser[†‡] Pietro P. Altermatt[†] Aidan Williams[‡] Alistair Sproul[†] Martin A. Green[†]
[†]Centre for Photovoltaic Devices and Systems
[‡]School of Computer Science and Engineering
The University of NSW, Sydney 2052, Australia
G.Heiser@unsw.edu.au, http://www.cse.unsw.edu.au/~gernot, Tel: +61 2 385 5156, Fax: +61 2 385 5995

ABSTRACT: This paper describes the use of three-dimensional (3D) device modelling for the optimisation of the rear contact geometry of high-efficiency silicon solar cells. We describe the techniques and models used as well as their limitations. Our approach is contrasted with previously published 3D studies of high-efficiency silicon solar cells. Results show that the optimum spacing is about 2/3 of that predicted by 2D simulations, and exhibits a much stronger dependence on contact spacing. The optimal value found is about 60 % of that of the present UNSW PERL cells, however, the possible efficiency gain is only about 0.1 % absolute.

1 INTRODUCTION

For the last three years a project has been under way at UNSW aiming at the comprehensive characterisation and optimisation of high-efficiency silicon solar cells with the aid of numerical modelling. The UNSW *passivated emitter, rear locally diffused* (PERL) high-efficiency silicon solar cells (Fig. 1) currently reach independently confirmed efficiencies of 24.0 % [1]. It is believed that with all design parameters fully optimised, this efficiency can be improved by a further 0.5–1.0 % absolute.

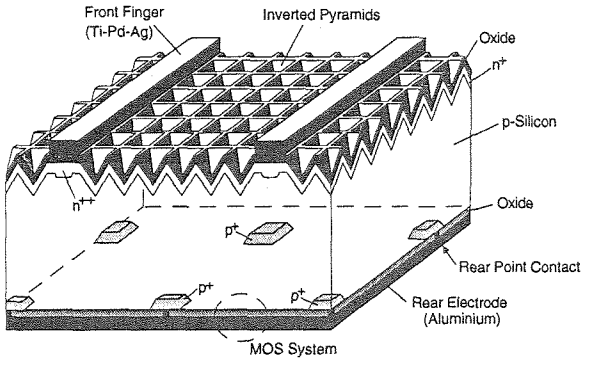

Figure 1: The UNSW PERL high-efficiency silicon solar cell.

The work performed over the last few years has provided us with a detailed understanding of the internal operations of PERL cells [2] and has made possible a quantitative analysis of limiting losses [3]. This analysis required a fine-tuning of our numerical models to a degree that we can now make accurate predictions of the effect of design modifications.

Most of our numerical modelling has, so far, been two-dimensional (2D). This is generally quite appropriate, as most features of PERL cells are essentially 2D. One of the main exceptions are the point-like rear contacts, which result in a three-dimensional (3D) majority carrier flow pattern in the base. For this reason, the base resistivity of PERL cells can only be accurately modelled in 3D. 3D modelling is also required in cases where the finite conductivity of the front metal contact grid and edge effects are relevant [4].

As base resistivity is an important factor determining the optimal design of the rear contact pattern, a numerical optimisation study of the base contact design of PERL cells requires the use of 3D simulation. This paper presents the results of such a study, and outlines the techniques used.

2 PREVIOUS WORK

We have previously published a 2D study of the rear contact geometry of PERL cells [5]. As explained above, 2D simulations cannot accurately determine the resistive losses in the base and are therefore only a rough approximation.

Several 3D simulations of high-efficiency silicon solar cells have been published before: Sterk and Glunz [6] simulated a similar structure, the ISE *local back surface field* (LBSF) cell, also with the aim of optimising the rear contact spacing. However, they made a number of simplifying assumptions, which limit the accuracy of their results. In particular, they only solved the semiconductor equations in the base and neglected the contribution of the minority carriers to the total current. Their results are in rough agreement with experimental data at large rear contact spacings, however, the experimental data show a much stronger dependence of the efficiency on the contact spacing than their simulation results, probably a result of the simplifications made. Sterk and Glunz find an optimum efficiency at a surprisingly large contact spacing of around 1 mm. This is about four times as large as the value presently used in PERL cells and seems to indicate that contact recombination plays a much more prominent role in ISE cells than in UNSW cells. This would result in strongly non-1D *minority* carrier flow in ISE cells, an effect that is ignored in their simplified model.

Another 3D study of the rear contact geometry, this time of cells PERC cells, i.e. cells without the rear contact diffusions, has been published by Schöfthaler et al. [7]. Their approach is based on Fourier analysis and is essentially analytical. They need to make similar assumptions as Sterk and Glunz, plus a few additional ones, like spatially homogeneous generation rates as well as assumptions on the maximum short circuit current, I_{sc}, and open circuit voltage, V_{oc}. Schöfthaler's method is attractive because it is computationally extremely cheap. However, it is intrinsically restricted to simple periodic geometries and does not allow modelling of general device characteristics of PERL cells.

Finally, Ohtsuka et al. have published a 3D optimisation study of the geometry of back-contact silicon solar cells [8]. They solve the full set of drift-diffusion equations. Their approach is, like Sterk and Glunz, based on a *finite difference* discretisation of the simulation domain which requires regular (so-

called *tensor-product*) meshes and, for geometries such as those of solar cells, results in very big grids. For a simulation domain of only $50\times50\times50\mu m^3$ (about two orders of magnitude smaller than ours) they end up with 187,500 grid points and require a supercomputer for their simulation. It is difficult to see how their approach could work on PERL cells.

Our work presents the first use of full 3D modelling, without simplifications, to such large devices as the UNSW PERL silicon solar cells.

3 THREE-DIMENSIONAL SIMULATIONS

Our simulations use the 1/2/3D device and circuit simulation package DESSIS developed at ETH Zurich [9]. We solve the full semiconductor equations in the whole device without any further simplifications. The simulations account for mobility degradation through impurity scattering and velocity saturation, doping-dependent minority carrier lifetimes, Auger recombination and recombination at metallised and oxidised surfaces. Band-bending effects resulting from fixed oxide charges and metal/silicon work function differences are fully included. Processing-dependent parameters are, as far as available, based on measured parameters of actual UNSW PERL cells, other parameters are based on fits to measured dark and illuminated I-V curves. The parameter values are summarised in Table 1.

wafer thickness	$370\,\mu m$
front contact spacing	F = $800\,\mu m$
rear contact spacing	R = variable
emitter doping	gaussian profile, $1\,\mu m$ deep, $5\times10^{18}cm^{-3}$, $200\,\Omega/\square$
emitter contact diffusion	$10^{20}\,cm^{-3}$
base doping	$1.4\times10^{16}\,cm^{-3}$ ($1\,\Omega cm$)
base contact diffusion	$5\times10^{19}\,cm^{-3}$
mobilities	doping dependent
bulk lifetime	Kendall formula, $\tau_{max} = 2\,ms$
Auger recombination	$C_n = C_p = 1.2\times10^{-30}\,cm^6s^{-1}$
surface recombination	
front	$S_e = S_h = 2000\,cm\,s^{-1}$
rear	$S_e = 50\,cm\,s^{-1}$, $S_h = 20\,cm\,s^{-1}$
rear surface band bending	
oxide charge	$Q_f = +1.3\times10^{11}q\,cm^{-2}$
barrier voltage	$V_b = -0.51\,V$
contact resistance	$\rho_c = 10^{-6}\,\Omega cm^2$

Table 1: Parameter values used in simulations.

Note that the values of the rear surface recombination velocity given in Table 1 are smaller than those actually measured for UNSW PERL cells ($S_n = 1000, S_p = 10\,cm/s$). However, we found indications for several kinds of traps with different ratios of electron/hole capture cross sections. Due to the injection-level dependent nature of surface recombination [5], different trap types are active under different operating conditions. We found that when using a single-trap model, the values given in Table 1 produce the best agreement between simulation and experiment. Details are subject of a forthcoming paper.

As edge effects and the resistivity of the metal fingers are not relevant to this study, symmetry arguments allow, without loss of accuracy, a restriction of the simulated volume to a region given as *half the front finger spacing* by *half the rear contact spacing* by *wafer thickness*, see Fig. 2.

This symmetry argument, however, only works if the rear contact spacing, R, is an integer fraction of the front contact spacing, F. For a PERL cell with $F = 800\mu m$, this restricts the possible values of R to the sequence

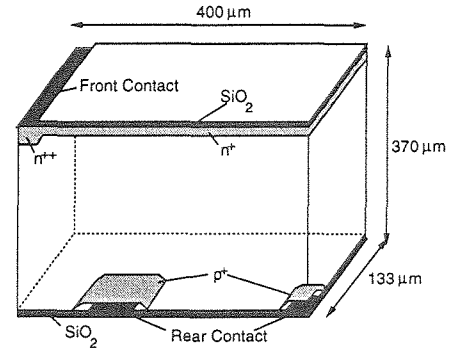

Figure 2: 3D simulation domain for a PERL cell with $F = 800\,\mu m$, $R = 267\,\mu m$.

$800, 400, 267, 200, 160, \ldots\,\mu m$, see Fig. 3. This is not a serious limitation as the allowed values are reasonably dense in the vicinity of $250\,\mu m$, the value of R used in present PERL cells.

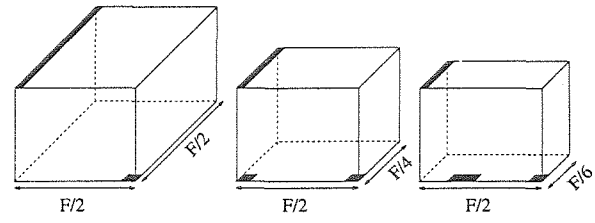

Figure 3: Simulation domains for different values of the contact spacing ratio F/R: 1 (left), 2 (middle), and 3 (right).

A particular difficulty of this study is that simulated cell characteristics, particularly I_{sc}, tend to be very sensitive to the density of the simulation mesh. A high density of mesh points is required around the rear contacts, as this is the area where the 3D effects are strongest. However, in order to keep the total mesh sizes reasonable, it is not possible to use the same high mesh density everywhere near the rear surface. This can lead to problems when comparing simulation results for different grid geometry, as these use different simulation meshes, with different location and extent of highly refined regions. Simulation meshes must be carefully designed to ensure that such results are really comparable.

case	*F/R of*			*simulated*
	contacts	*domain*	*mesh*	I_{sc} *[mA/cm²]*
111	1	1	1	41.101
777	7	7	7	41.091
171	1	7	1	41.075
177	1	7	7	41.078

Table 2: Influence of mesh on simulated I_{sc}.

Table 2 shows simulations performed to investigate the extent of this *discretisation error*. The cases labelled "111" and "777" are normal simulations for $F/R = 1$ and $F/R = 7$ respectively, they differ in I_{sc} by only $10\,\mu A/cm^2$, or 0.02 %. "171" and "177" are special test cases. Both use the smaller simulation domain corresponding to $F/R = 7$, while using only one rear contact (as for the $F/R = 1$ case). They differ in that "171" uses the mesh of the $F/R = 1$ simulations (restricted to the smaller domain) while "177" uses the $F/R = 7$ mesh. The resulting I_{sc} values differ by $3\,\mu A/cm^2$, or 0.007 %. We can therefore be assured that the discretisation error will not influence our results.

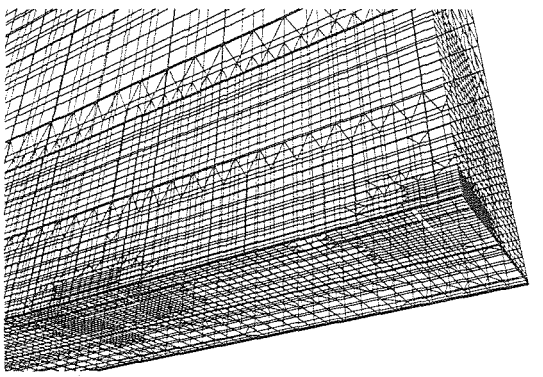

Figure 4: Partial view of simulation mesh for $F/R = 7$, consisting of 122,067 points. The picture shows the mesh on the outside of the simulation domain viewed from the bottom right-hand corner. The refinement around two of the contacts can be seen.

The resulting mesh sizes varied between 60,000 and 200,000 points, depending on the value of F/R; Fig. 4 shows a typical example. CPU time requirements for the simulation of a full I-V curve were of the order of 3–5 days on a 60 MHz Sun SPARCstation 20 with 256 Mbyte of RAM.

The present PERL design uses a rear contact spacing of 250μm, where the contacts are $10\times10\mu m^2$ large, corresponding to a metallisation fraction of 0.14 %. While our simulations show that the contact size is not a limitation in present cells and smaller contacts could produce efficiency advantages, particularly at smaller spacings, technical limitations presently prevent the use of smaller contacts. In our study we therefore fixed the rear contact size at $10\times10\mu m^2$.

For comparison, we also performed 2D simulations. There are two ways to perform a 2D simulation "corresponding" to a 3D one: A cross section of a 3D domain results in a 2D model of a device with rear contact fingers of a width identical to the width of the 3D point contacts (10 μm), and hence a much larger metallisation fraction (3.75 % vs. 0.14 % for $F/R = 3$). Alternatively, the metallisation fraction can be kept constant, resulting in a 2D model with very narrow fingers (0.375 μm vs. 10 μm for $F/R = 3$). As the metallisation fraction determines the current crowding and thus the dominating resistive losses within the base, we modelled both of these extreme cases.

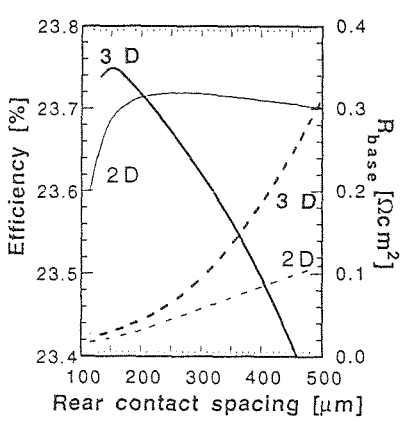

Figure 5: Efficiency and base resistivity of PERL cell according to 2D and 3D models, both using the same metallisation fraction.

4 RESULTS

Fig. 5 shows the calculated AM1.5G PERL cell efficiency as a function of the rear contact spacing. It can be seen that the 3D model predicts an optimum efficiency at a contact spacing of around 150 μm, while 2D simulations predict an optimum spacing of about 250 μm (consistent with [5]). The 3D results show a much stronger decrease of efficiency with larger contact spacing. This is a consequence of the increased base resistance resulting from the crowding of the majority current in the vicinity of the rear contacts, as can be seen in Fig. 6: 2D simulations, even when using the same metallisation fraction as in 3D, significantly underestimate the base resistance. The 2D value of the base resistance is only weakly dependent on the metallisation fraction.

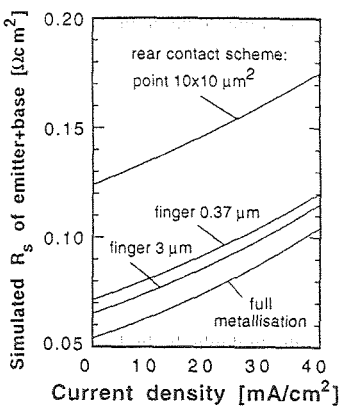

Figure 6: Internal series resistance of a PERL cell with $R = 267\ \mu$m according to 2D and 3D models.

The underestimation of the base resistance in 2D results in an overestimation of the fill factor: Fig. 7 shows that in 3D the fill factor reduces strongly with increasing contact spacing, while in 2D it is essentially constant.

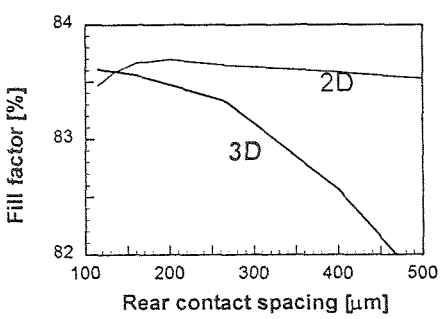

Figure 7: Fill factor of a PERL cell as a function of rear contact spacing according to 2D and 3D models (same metallisation fraction), ignoring metal resistance.

At small contact spacings the efficiency drops due to a decrease in V_{oc} as shown in Fig. 8. The drop in V_{oc} results from an increase in recombination, an effect of the larger fraction of the rear surface being covered by p^+ diffusions at smaller contact spacings. This effect is *overestimated* by 2D simulations. Consequently, 2D simulations underestimate PERL cell efficiency at small contact spacings (compare Fig. 5).

Note that due to the extremely low recombination losses in PERL cells, our simulations showed negligible dependence of I_{sc} on the contact spacing.

The combination of the effects discussed above results in a shift of the maximum of the efficiency as obtained from 2D

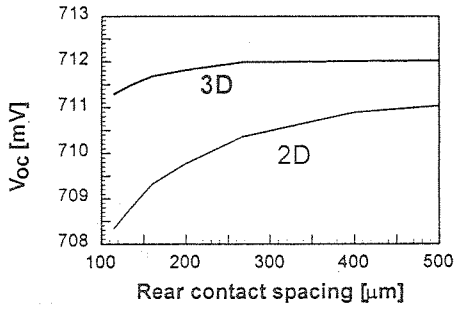

Figure 8: V_{oc} of a PERL cell as a function of rear contact spacing according to 2D and 3D models (same metallisation fraction).

modelling to larger values than in 3D. The actual maximum values are actually quite close for PERL cells, with the 3D value being slightly higher. These effects will balance out differently if another substrate resistivity or peak concentration of the p^+ diffusions is chosen. In cases where base resistivity is more important, a 2D (finger) contact scheme may produce a higher efficiency than 3D (point) contacts. Accurate predictions, however, can only made with 3D simulations.

The predicted optimum contact spacing of around 150μm is about 60 % of the value used in present UNSW cells, with a predicted efficiency loss of 0.1 % absolute due to the larger contact spacing. However, it needs to be pointed out that material stress at the Si/SiO_2 interface near the metal contacts introduces crystal dislocations which travel up to several micrometres into the bulk during high-temperature processing. Not much is known about the extent and effect of these dislocations. For this reason they could not be included in our numerical models. As the relative abundance of such dislocations increases with the number of contacts, their effects would be most prominent at high F/R values. This should shift the optimum rear contact spacing to somewhat higher values than obtained from our numerical models.

In summary it can be said as a result of this study that the spacing of the rear contacts of PERL cells is somewhat larger, although close, to the optimum. An efficiency improvement of at most 0.1 % absolute can be gained from a modification of the rear contact geometry.

REFERENCES

[1] J. Zhao, A. Wang, P. P. Altermatt, S. R. Wenham, and M. A. Green. 24 % Efficient silicon solar cells. In *1st World Conf. Photovoltaic Energy Conversion*, pages 1477–80, Waikoloa, HI, USA, December 1994. IEEE.

[2] S. J. Robinson, S. R. Wenham, P. P. Altermatt, A. G. Aberle, G. Heiser, and M. A. Green. Recombination rate saturation mechanisms at oxidised surfaces of high-efficiency silicon solar cells. *J. Appl. Physics*, 1995. To appear.

[3] A. G. Aberle, P. P. Altermatt, G. Heiser, S. J. Robinson, A. Wang, J. Zhao, U. Krumbein, and M. A. Green. Limiting loss mechanisms in 23-percent efficient silicon solar cells. *J. Appl. Physics*, 77:3491–504, 1995.

[4] P. P. Altermatt, G. Heiser, J. Zhao, A. Wang, and M. A. Green. Analysis and minimisation of resistive losses in high efficiency Si solar cells by combining measurements with numerical modelling. In *Proc. 13th European Photovoltaic Sol. Energy Conf.*, Nice, France, October 1995.

[5] A. G. Aberle, G. Heiser, and M. A. Green. Two-dimensional numerical optimisation study of the rear contact geometry of high-efficiency silicon solar cells. *J. Appl. Physics*, 75(10):5391–405, 1994.

[6] S. Sterk and S. Glunz. Simulation in high efficiency solar cell research. In *Proc. 5th Int. Conf. Simul. Semicond. Dev. and Proc.*, pages 393–6, Vienna, Austria, 1993. Springer Verlag.

[7] M. Schöfthaler, U. Rau, W. Füssel, and J. Werner. Optimization of the back contact geometry for high efficiency solar cells. In *Proc. 23rd IEEE Photovoltaic Specialists Conf.*, pages 315–20, Louisville, KY, USA, 1993. IEEE.

[8] H. Ohtsuka, Y. Ohkura, T. Uematsu, and T. Warabisako. Three-dimensional numerical analysis of contact geometry in back-contact solar cells. *Prog. Photovoltaics*, pages 275–85, 1994.

[9] ISE Integrated Systems Engineering AG, Zurich, Switzerland. *DESSIS 1.3.6: Manual*, 1994.